④

Inertial Upper Stage Thermal Test Program

D. J. SPENCER and H. A. BIXLER
Aerophysics Laboratory ·
Laboratory Operations
The Aerospace Corporation
El Segundo, CA 90245

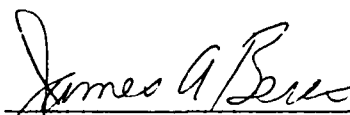12 April 1989

AD-A208 052

This report was submitted by The Aerospace Corporation, El Segundo, CA 90245, under Contract No. F04701-85-C-0086-P00016 with the Space Systems Division, P.O. Box 92960, Los Angeles, CA 90009-2960. It was reviewed and approved for The Aerospace Corporation by W. H. Drake, Principal Director, Upper Stages, Space Launch Operations. Lt Robert Day, SSD/CLUE, was the Air Force project officer.

This report has been reviewed by the Public Affairs Office (PAS) and is releasable to the National Technical Information Service (NTIS). At NTIS, it will be available to the general public, including foreign nationals.

This technical report has been reviewed and is approved for publication. Publication of this report does not constitute Air Force approval of the report's findings or conclusions. It is published only for the exchange and stimulation of ideas.

ROBERT DAY, Lt, USAF
Project Officer
SSD/CLUE

JAMES A. BERES, Lt Col, USAF
Director, AFSTC West Coast Office
AFSTC/WCO

REPORT DOCUMENTATION PAGE

1a. REPORT SECURITY CLASSIFICATION	1b. RESTRICTIVE MARKINGS
Unclassified	

2a. SECURITY CLASSIFICATION AUTHORITY	3. DISTRIBUTION / AVAILABILITY OF REPORT
2b. DECLASSIFICATION / DOWNGRADING SCHEDULE	Approved for public release; distribution unlimited.

4. PERFORMING ORGANIZATION REPORT NUMBER(S)	5. MONITORING ORGANIZATION REPORT NUMBER(S)
TR-0086A(2464-01)-1	SD-TR-89-26

6a. NAME OF PERFORMING ORGANIZATION	6b. OFFICE SYMBOL (If applicable)	7a. NAME OF MONITORING ORGANIZATION
Laboratory Operations The Aerospace Corporation		Space Systems Division

6c. ADDRESS (City, State, and ZIP Code)	7b. ADDRESS (City, State, and ZIP Code)
El Segundo, CA 90245	Los Angeles Air Force Base Los Angeles, CA 90009-2960

8a. NAME OF FUNDING / SPONSORING ORGANIZATION	8b. OFFICE SYMBOL (If applicable)	9. PROCUREMENT INSTRUMENT IDENTIFICATION NUMBER
		F04701-85-C-0086-P00016

8c. ADDRESS (City, State, and ZIP Code)	10. SOURCE OF FUNDING NUMBERS			
	PROGRAM ELEMENT NO.	PROJECT NO.	TASK NO.	WORK UNIT ACCESSION NO.

11. TITLE (Include Security Classification)

Inertial Upper Stage Thermal Test Program

12. PERSONAL AUTHOR(S)
Spencer, Donald J., and Bixler, Henry A.

13a. TYPE OF REPORT	13b. TIME COVERED FROM _____ TO _____	14. DATE OF REPORT (Year, Month, Day) 1989 April 12	15. PAGE COUNT 32

16. SUPPLEMENTARY NOTATION

17. COSATI CODES			18. SUBJECT TERMS (Continue on reverse if necessary and identify by block number)
FIELD	GROUP	SUB-GROUP	IUS → Silica phenolic, Solid propellant, Thermal testing,
			EPDM Grafoil seal, Rocket engines,
			Viton Thermal-protection materials,

19. ABSTRACT (Continue on reverse if necessary and identify by block number)

An extensive thermal testing program was performed in an arc tunnel facility in support of an IUS second-stage solid rocket motor (SRM) requalification activity. A three-phase laboratory thermal study of failure scenarios resulted in the following items. First, bursting of the SRM environmental closure was pressure rather than temperature dependent, which allowed full-scale cold-gas simulation of the closure burst sequence. Secondly, arc tunnel ablation measurements of EPDM, a thermal insulative rubber material covering the SRM ignitor housing, were made in both convective and radiative heater environments under varied sample vibration levels to simulate the measured motor vibration environment. The EPDM radiation recession rate scaled to the SRM environment (6000°R, 600 psia peak chamber conditions) was 3.7 mil sec^{-1}, in agreement with later static test firing measurements, indicating the motor case heat-transfer environment near the ignitor housing to be basically and remarkably purely radiative and virtually uninfluenced by char loss due to vibration or convection. Thus EPDM showed itself to be a very effective SRM thermal protection material. Finally, hot-gas leakage past a grafoil seal emerged as

20. DISTRIBUTION / AVAILABILITY OF ABSTRACT	21. ABSTRACT SECURITY CLASSIFICATION
☒ UNCLASSIFIED/UNLIMITED ☐ SAME AS RPT. ☐ DTIC USERS	Unclassified

22a. NAME OF RESPONSIBLE INDIVIDUAL	22b. TELEPHONE (Include Area Code)	22c. OFFICE SYMBOL

DD FORM 1473, 84 MAR   83 APR edition may be used until exhausted.   SECURITY CLASSIFICATION OF THIS PAGE
All other editions are obsolete.

19. ABSTRACT (Continued)

the most likely SRM failure scenario. Arc tunnel testing of silica phenolic thermal
insulation candidates to protect the SRM nozzle titanium Techroll housing resulted
in verification of a satisfactory design concept which has since been implemented
in successful flight hardware.

PREFACE

The authors wish to express appreciation to Dick Hartunian, Syl Lafazan, Ernie Stampfl, Ernie Scheyhing, Don Lapedes, Connie Pel, Mike Fukuda, and I-Shih Chang for their contributions and directions given during the reported test program. The photographic documentation of John Rush is also gratefully acknowledged. The efforts of Robert Cook and William Hansen were essential to arc tunnel operation. The assistance of Sheldon Rubin and Dave Ross in sample vibration measurements is also appreciated.

1

CONTENTS

FIGURES

TABLES

I. INTRODUCTION

The uncommanded second-stage rocket motor (SRM-2) thrust vector deviation, experienced during the April 1983 IUS orbit boost flight of the TDRS-A payload, resulted in tumbling and precipitated a setback in the national space program. A concerted effort to uncover a most probable failure scenario and demonstrate suitable design correction was immediately implemented, culminating in the successful SIS-IUS launch of January 1985.[1,2] An extensive thermal testing program was performed in The Aerospace Corporation laboratories that contributed heavily to this successful requalification activity in support of the Air Force and the concerned contractors, BAC and UTC-CSD. A total of four full-scale static test firings were also performed at AEDC, guided by the laboratory thermal test program under consideration here. Details of the IUS launch vehicle characteristics and corrective action taken in requalification are well documented in the literature.[3-6]

Three basic failure scenarios were suggested as being responsible for the aberrant behavior of the thrust vector control system. All scenarios focussed on methods of overheating with subsequent failure of the high-pressure silicone-oil-filled Techroll annular ring member, which allowed nozzle swivel movement. The first failure scenario involved bursting of the rubberized Kevlar cloth seal bonded to the upstream nozzle face (called environmental closure) at the instant of ignition. This could possibly damage the rocket nozzle slightly downstream of the throat, allowing hot motor exhaust gases to penetrate the Techroll gimballing ring, resulting in failure. The second scenario involved fragments from the breakup of a failed ignitor housing chipping pieces off the nose cap wing portion of the gimbal nozzle, resulting in loss of thermal protection to the Techroll ring. The third scenario involved hot-gas leakage through a grafoil seal ring separating the throat and exit cone portions of the nozzle. This would allow heating and subsequent failure of the Techroll ring. See Fig. 1 for a cutaway drawing of the IUS motor and second-stage parts locations associated with these three potential failure modes. Discussion of the thermal testing in the arc tunnel associated with each of these failure scenarios will be taken up in sequence.
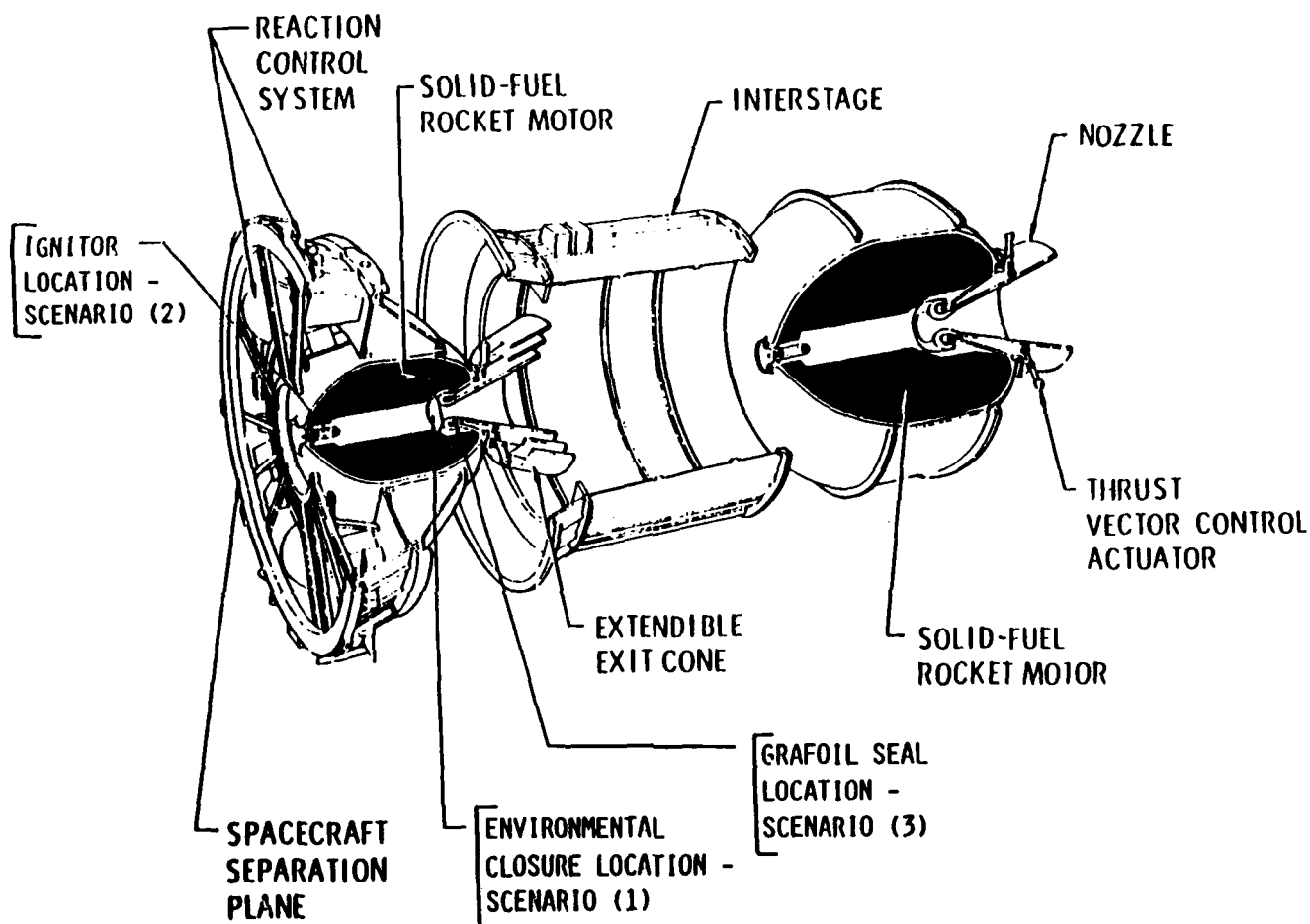
Fig. 1.   Cutaway drawing of inertial upper stage, highlighting three failure-
scenario locations.

II. ENVIRONMENTAL CLOSURE THERMAL BURST

The interior of the IUS SRM-2 motor was protected from the environment prior to firing by means of a rubberized Kevlar cloth seal which was bonded to the upstream nozzle face. This seal burst immediately after motor ignition ($\sim$ 5 msec) and could possibly have produced damage from high-velocity closure fragments in the rocket nozzle, slightly downstream of the nozzle throat, upon rupture. Breakage of the nozzle surface could allow hot exhaust gases to penetrate to the Techroll gimballing ring employed in the movable nozzle, resulting in failure. The closure burst mechanism was initially thought to be thermal in nature, since SRM combustion occurs at 6000°R. Arc jet heating tests of Kevlar test samples were initiated to verify the thermal burst hypothesis and observe the nature of the burst preliminary to more complete testing.

One-inch-square test samples were cut from a 15-1/2-in.-diam, 0.016-in.-thick rubberized Kevlar cloth diaphragm previously used in pressurized burst tests. The first three samples were clamped in place to cover a 1/2-in.-diam hole at the rear of a 1/2-in.-thick graphite sample holder through which the 1/2-in.-diam hole had been drilled. The sample holder hole was counter-bored on the front side to a 3/4 in. diam for jet entrainment. The test samples were placed in position in the arc tunnel test section a distance 2.5 in. downstream of the exit face of a 1/2-in.-diam subsonic nozzle attached to an arc heater. To initiate the sudden heating of the test sample, a water-cooled jet deflector, initially positioned between the nozzle face and the test sample holder, was rapidly rotated out of the jet after achievement of previously calibrated test conditions.

A fourth test involved attachment of the test sample by means of Dexter-Hysol Epoxy EA 901/B-1 (cured at 150°F for 2 hours and at room temperature for 24 hours as in the actual IUS SRM application) to the rear surface of the sample holder, again covering the 1/2-in.-diam hole. The sample holder was then rotated 180° to provide jet impingement directly on the cloth and splash heating of the annular glue joint of the sample. The nozzle sample displacement distance was maintained at 2.5 in. The N_2 plasma jet stagnation temperatures were 5360°R (tests 1, 2, and 4) and 8260°R (test 3). Test results are tabulated in Table I.

9

Table I. Experimental Data for Arc-Jet-Heated Kevlar Cloth

Test No.	Temp. (°R)	Burn-Through Time (sec)
1	5360	1.0
2	5350	0.9
3	8260	0.8
4	5360	1.4[a]

[a]Epoxy heating test.

This test series established that burn-through time for unpressurized cloth was of order 1 sec. Initial expectations placed the time at as low as 5 msec. High-speed photographs of the burn-through tests showed a general dissolution and breakup of the material from the center of the diaphragm radially outward to the edges. The diaphragm was not punched out cleanly as if excised by a cookie cutter.

Thus laboratory thermal studies bearing on scenario (1) established that bursting of the environmental closure was pressure rather than temperature driven, which allowed full-scale cold-gas simulation of the closure burst sequence. High-speed camera recording of these latter tests established the closure-flap forces on the exit cone to be potentially damaging. A cleaner, four-petal defoliating closure burst was developed in this study and was implemented in the vehicle design, thus minimizing this potential motor performance threat. This scenario was deemed less probable through this work.

III. EPDM AND VITON ABLATION CHARACTERISTICS

Scenario (2) focussed attention on the integrity of the head-end-mounted ignitor housing und. thermal load. The scenario envisioned a possible burn-through of the ignitor insulative material (EPDM-Neoprene rubber) during motor operation follow-d by ejection of breakup and melt fragments into the motor, resulting in nozzle damage before exiting the throat. See Fig. 2 for a cross-sectional drawing of the IUS SRM-2 ignitor. The EPDM ignitor insulation material is vulcanized to the aluminum ignitor housing, hence is free of interface voids. The integrity question for this material then centers on its ablation characteristics in the high-temperature, high-pressure (6000°R, 600-psi peak), high-heating-rate environment of the rocket motor combustor. Arc tunnel ablation measurements of the EPDM material were therefore made in both radiative and convective heating environments.

A. RADIATION HEATING

The test configuration for the radiation tests is shown in cross-sectional plan view from above in Fig. 3 and in photographic form from the side in Fig. 4. The arc jet emerged from a 1/2-in.-diam cooled copper nozzle and splashed against the back side of a 2-in.-diam 4D weave carbon-carbon disk held in position 1-1/2 in. downstream of the nozzle exit plane. The arc heater operated typically at 19-psia plenum pressure with 6 g sec^{-1} N_2 as the working gas, and with 220 kW of electrical power (400 V, 550 A). The nozzle face required a water-cooled shield to protect internal O-rings against back-side radiator radiation heating. A removable shutter consisting of either a 1/2-in.-thick graphite slab or water-cooled titanium plate was inserted from the side between the radiator and the sample. The radiator was heated 20 sec to thermalize before the movable shutter was rapidly removed to initiate radiation loading of the sample positioned 1 in. from the radiator front face. The test sample was supported in position by a sting attached to an axial electro-mechanical vibrator, and the sample axial acceleration was measured with a piezo-electric accelerometer. Both radiator and sample surface temperatures were measured pyrometrically. The test section was purged with N_2 to ensure an inert environment for these tests.

Fig. 2.   IUS SRM-2 ignitor.

EMI SHIELD

MOVABLE
GRAPHITE
PLATE
SHUTTER

RADIATOR

WATER
COOLED
SHIELD

ACCELEROMETER

VIBRATOR
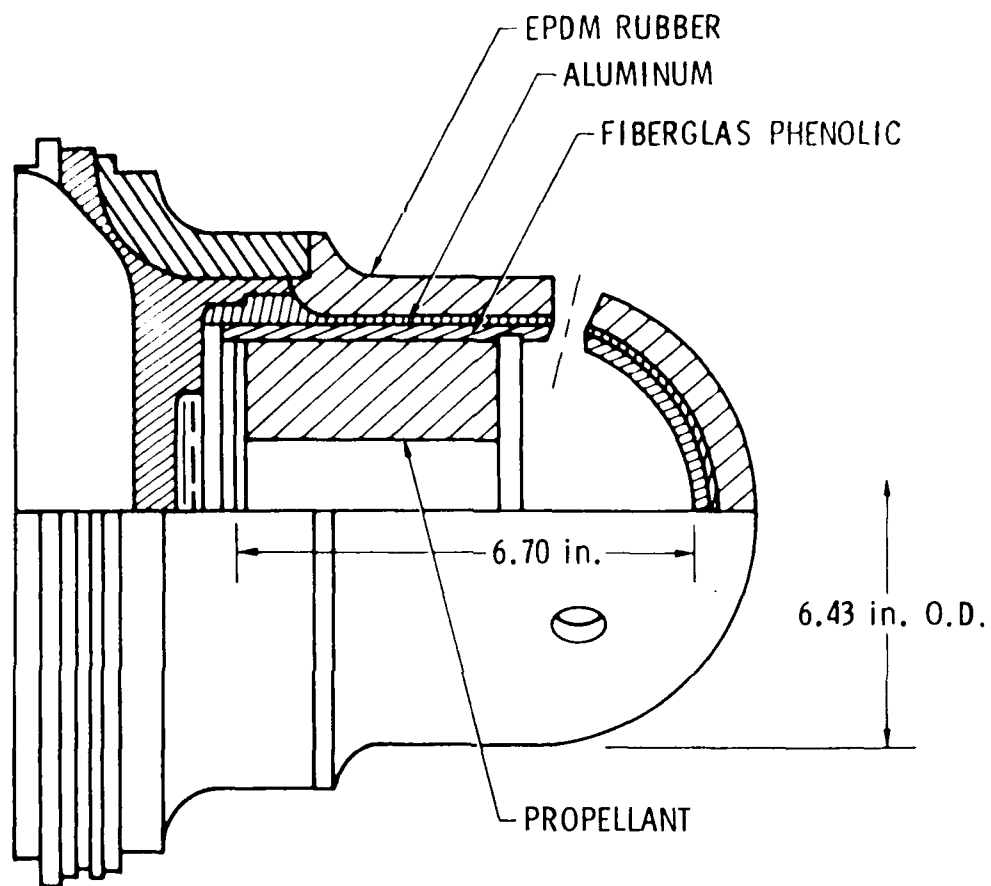STING

EPDM
TEST
SAMPLE

JET
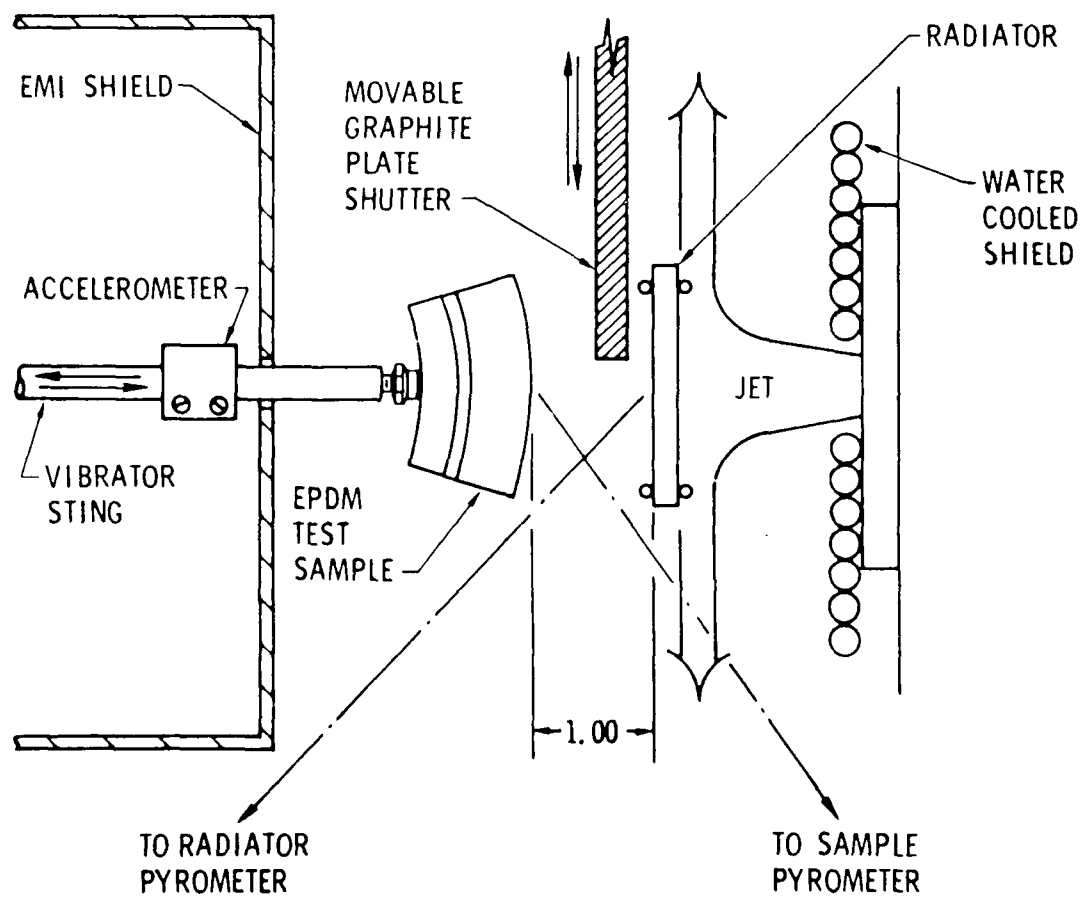
1.00

TO RADIATOR
PYROMETER

TO SAMPLE
PYROMETER

Fig. 3.   Radiation testing array—plan view.

Fig. 4.   Photograph of radiation testing array--side view.

Samples made from the cylinder, spherical cap, and skirt adapter portions of an EPDM ignitor cover were tested, with no differences noted between the behavior of the three configurations. The bulk of the data was obtained with samples made from the cylindrical portion of the ignitor cover. Test results for six tests are tabulated in Table II. The radiator was quite uniform in temperature across its surface and was reduced only about 100°R at the edges from the temperature at the center. The average and centerline view factors associated with the radiator as seen from the test sample face were computer-calculated for the geometry employed.[7] The sample centerline radiant heat flux was calculated from the radiator temperature and the centerline view factor for an assumed emissivity of 1. The column labeled $\dot{Q}$ (RAD)/$\dot{Q}$ (MOTOR) provides the ratio of the test sample centerline radiation heating rate to the radiant heating rate experienced at the ignitor surface immersed in the 6000°R blackbody radiating combustion gases of the rocket motor. The ideal ratio of 1 was not attainable with this facility, but at the highest test conditions the ratio was 0.54, which was considered a close enough approximation for useful testing.

The effects of motor vibration on material recession rate through char flaking were a matter of concern in these tests, so the sample support sting was attached to an axial vibrator and piezo-electric accelerometer for monitoring and controlling the sample vibration level during test. The acceleration reported from AEDC static-firing measurements was 0.05 to 0.1 g_{rms} over a 20- to 20,000-Hz bandwidth. The arc tunnel test-stand ambient axial level was measured at 0.11 g_{rms} over a 20- to 1000-Hz bandwidth and 0.27 g_{rms} over a 20- to 10,000-Hz bandwidth, indicating the presence of high-frequency components. Thus the test ambient level slightly exceeded the static firing values and therefore represented a good test environment without superimposed vibration. However a more severe vibration condition, 5 g_{rms} at 340 Hz, was imposed on the tests of samples 4, 5, and 6 in order to disclose the influence of that environment upon the ablation rate.

The measured recession rates for ~ 60 sec run times are presented for each test sample in two ways. (1) The EPDM material recession rate measured at the sample centerline down to the region where the material is virgin, i.e., at the point of onset of material depolymerization. This is the deepest material physico-chemical change penetration depth; it required scraping both

15

Table II. EPDM Radiation Test Results
[View Factor ℓ (at EPDM) 0.50[a]]

Radiator Temp. (°R)	Run Time (sec)	$\dot{q}_\ell$(RAD) (Btu ft⁻² sec⁻¹) ($\varepsilon = 1$)	$\dot{Q}$(RAD)/$\dot{Q}$(MOTOR)	Vibration[b] (g_rms)	Maximum Char Temp (°R±10°R) at Char Loss	$\dot{S}(\ell)$ to Virgin EPDM (mil sec⁻¹)	q^*_{RAD}[c] (Btu lb⁻¹)	$\dot{x}$ to Spongy Char Layer (mil sec⁻¹)	$\dot{x}$ to Spongy Char Projected for Static Firing (mil sec⁻¹)	Char Losses, Time(sec)/No.
+280 6160-30	60	340	0.54	0.11-0.27	4308	2.9	12,000	2.0	3.7	>60 / 0
>6160	59	340	0.54	0.11-0.27	4218	2.9	12,000	1.9	3.5	>60 / 0
+50 5710-300	60	250	0.40	0.11-0.27	4119	2.5	9,200	1.5	3.8	>60 / 0
+200 5960-150	60	300	0.47	5.0	4002	2.9	11,600	2.1	4.4	27.2 60 / 2
+180 5530-570	60	220	0.35	5.0	4020	2.7	7,300	1.9	5.3	17.4 61 / 2
+50 5610-150	57.5	240	0.37	5.0	4056	3.3	6,800	2.2	6.6	15.4 25.2 59 / 3

NOTE: ℓ = centerline.

[a] Sample avg. view factor = 0.37.

[b] 0.11 g_rms (20-1000 Hz ambient), 0.27 g_rms (20-10,000 Hz ambient). Tunnel ambient acceleration level is only slightly higher than the axial level reported from static firings (0.03-0.1 g_rms). 5.0 g_rms (340 Hz) superimposed on ambient level by axial vibrator in tests 4, 5, and 6.

[c] $q^*_{RAD} = (\dot{q}_{RAD} - \dot{q}_{SR})/\rho\dot{S}$.

16

the low-density frothy char layer and denser spongy char layer in order to make the measurement. (2) The EPDM material recession rate measured at the sample centerline down to the spongy char region lying above the virgin material, i.e., the interface between the low-density frothy char layer and the more dense spongy char region. It should be noted that the material sample as a whole did not recede under radiant heating, because the frothy char expanded typically 1/2 in. or more within a few seconds toward the radiator and remained intact throughout the test duration for tests 1, 2, and 3. This low-density char is easily brushed aside to make the recession measurements to the more dense spongy char layer, or deeper (typically ~ 0.050 in.) to the virgin material.

The projected recession rate for a static-firing case may be made from these data, assuming a linear dependence of recession rate on radiant heating rate. The projected recession rate to the spongy char level for each test is listed in the column so labeled in Table II. The results for tests 1 through 3 are 3.7, 3.5, and 3.8, respectively. The comparable measured EPDM recession rate on an ignitor which was water-quenched after firing to inhibit heat soak was 3.7 mil sec^{-1}, in good agreement with the projections.

Samples tested in runs 4, 5, and 6 were subjected to shaker-induced vibration a factor ~ 20 times the ambient tests and a factor ~ 50 greater than the static test vibration environment. The last column of Table II lists the number of char losses during the test duration for these and the three preceding tests. No char flakes were lost in the first three tests, whereas 2, 2, and 3 flakes were lost during tests 4, 5, and 6, respectively, as a result of the added vibrational load. As each char flake, which measured the full sample size in height and width and from ~ 1/4 in. to 3/8 in. thick, would fall off, it would be rapidly replaced (~ few seconds) by regrowth from the newly exposed surface to the previous ~ 1/2 in. thickness; thus, char loss was not catastrophic. The net effect of this harsher condition may he easily seen by comparing the projected recession rates, 4.4, 5.3, and 6.6 for tests 4, 5, and 6, respectively, to the ~ 3.7 values obtained for the ambient vibration case. The principal value of these enhanced-vibration tests is to indicate that the frothy, low-density char is quite strong; and even when removed under heavy shaking it is rapidly replaced with only a moderate increase in recession rate, not an overwhelming increase. It should also be observed that

17

larger surface area samples, or even more so, larger contiguous surfaces such as those present in the EPDM covering of the ignitor, would tend to hold the low-density char with greater tenacity than observed in these tests.

B.   CONVECTION HEATING

Removal of the radiator and shutter from the test section and replacement of the vibrator and sting support for the samples with a simple sample holder enabled performance of conventional subsonic arc jet splash tests. See Fig. 5 for a photograph of a test in progress. Test samples of EPDM and Viton, 2 in. in diameter × 1/4 in. thick, were tested at "low" and "high" convective heating rate conditions, i.e., 84 Btu ft^{-2} sec^{-1} and 410 Btu ft^{-2} sec^{-1} cold-wall centerline heating rates $\dot{q}_{CW}$ as measured by a slug calorimeter array. Sample front-face temperature, T_{HW}, was measured pyrometrically to determine the hot-wall heating rate $\dot{q}_{HW}$ and the sample radiation heat loss $\dot{q}_{SR}$. Arc heater conditions were the same for both convective and radiation heating tests. Run times ranged from 5 to 15 sec.

The measured recession rates, $\dot{S}$, and calculated ablation figures of merit, Q^*, together with the pertinent test data for convection heating studies, are presented in Table III. The recession rates for EPDM are smaller than the comparable rates for Viton by a factor ~ 2 over the range tested. In addition the thermal dissipation capability per unit mass loss, Q^*, for EPDM is larger by a factor ~ 2.5 than the Q^* for Viton over the range tested. Thus EPDM clearly emerges as the superior ablative heat protection material in these tests.

This series of tests was performed to understand EPDM behavior in either radiative or convective heating environments. It was unknown at the time of testing which heating mode dominated at the ignitor housing heat-protection covering. The test series included Viton in comparison with EPDM, because Viton was employed as the housing material surrounding/protecting the Techroll Seal at the nozzle. In the failure scenario under consideration, the failed ignitor housing could chip pieces of the nose cap wing portion of the gimbal nozzle, resulting in exposure of the Viton housing. Thus the ablative properties of Viton were needed to ascertain the extent of protection the Viton afforded the Techroll Seal in such an event.
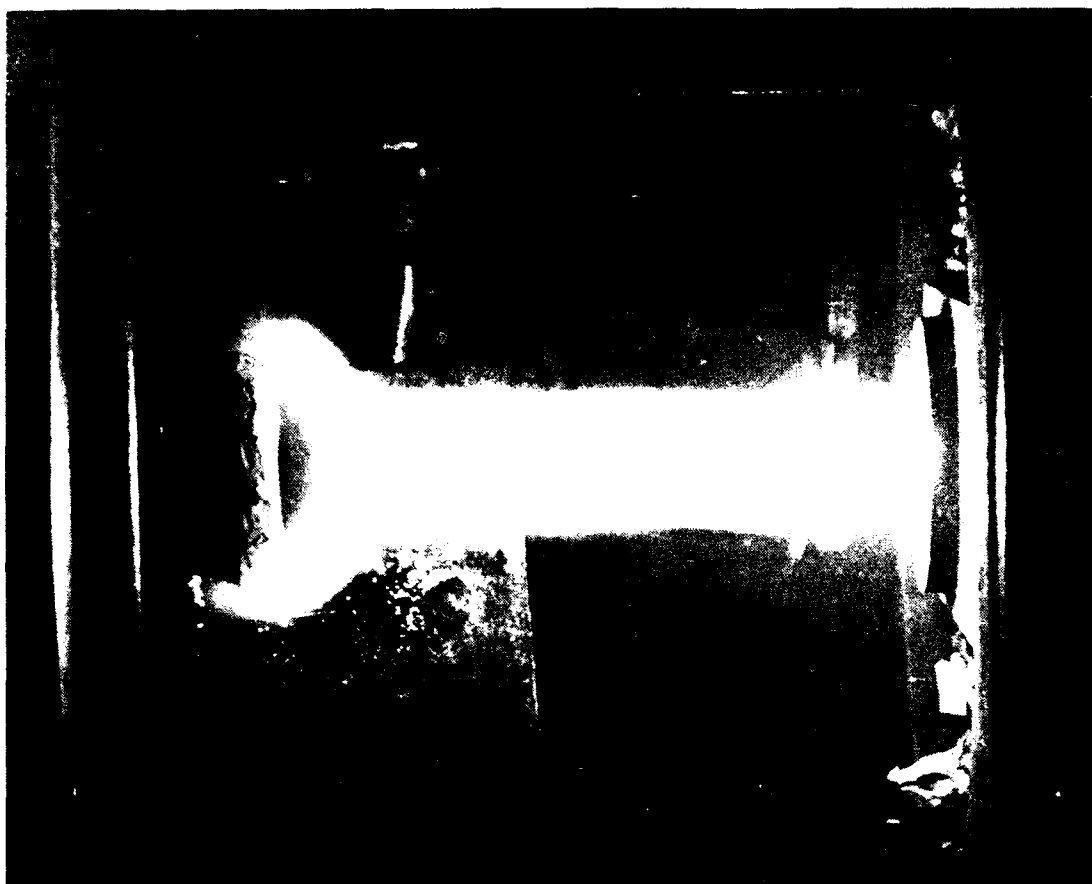
Fig. 5. Subsonic arc jet convection heating test of EPDM sample
(84 Btu ft^{-2} sec^{-1} centerline heating rate).

Table III. Arc-Jet-Heating Test Results, EPDM and Viton[a]

Material	T_o (°R)	T_{HW} (°R)	$\dot{q}_{CW}/\dot{q}_{HW}$[b] (Btu ft^{-2} sec^{-1})	$\dot{q}_{SR}$ (Btu ft^{-2} sec^{-1})	$\dot{S}$ (mil sec^{-1})	Q^*_{conv}[c] (Btu lb^{-1})
EPDM	~ 4500	2660	84/40	20	3.4	990
EPDM	~ 4500	2560	84/43	18	3.8	1100
EPDM	~ 4900	3360	410/142	52	15	1030
EPDM	~ 4900	3380	410/140	53	17	880
Viton	~ 4500	2460	84/44	15	7.5	410
Viton	~ 4500	2460	84/44	15	7.3	420
Viton	~ 4900	3360	410/142	52	25	380
Viton	~ 4900	3372	410/141	52	24	390

[a] Test results for nitrogen jet in ambient air. Recession rates are 10% smaller for tests in an N_2-purged test section.

[b] $\dot{q}_{HW} = \dot{q}_{CW} (T_o - T_{HW})/(T_o - T_{CW})$

[c] $Q^*_{conv} = (\dot{q}_{HW} - \dot{q}_{SR})/\rho\dot{S}$

EPDM and Viton were further compared at one test condition for performance under radiative heating. The test results for this comparison are presented in Table IV. The measured recession rates differ for these tests by a factor ~ 2.3, again in favor of EPDM. The Q^* ratio is ~ 3, again indicating the superiority of EPDM.

C. SUMMARY

Table V summarizes the EPDM-Viton Comparison Study in terms of recession rates and Q^* for both convective and radiative heating at nominally the same net heating rates. EPDM emerges as superior to Viton for both heating modes. Both materials handle radiative heating much better than convective heating, as evidenced by both recession rates and mass loss per unit energy absorbed, by about a factor of 10 for EPDM and a factor of 7.5 for Viton. This is due to the fact that char is swept away as scintillating sparklers under the shear stress associated with convection heating, whereas under radiative heating the char remains intact. The maximum shear stress experienced by the models in these tests was calculated to be of order 0.2 lb ft^{-2}. Thus a very small shear stress can prevent low-density char formation.

Comparison of the arc jet test results with the AEDC static test firing data was initially not possible, because heat soak had obscured post mortem evaluation of the previous 29 developmental and qualification static test firings of the IUS SRMs. Thermal shock testing in the arc tunnel through 1 min arc heating followed by water quench showed that the 3D carbon-carbon SRM-2 nozzle throat material experienced no cracking and established that a factor-of-30 improvement in cool-down time was obtainable. The four subsequent AEDC static test firings performed in association with this program were therefore water-quenched at burn termination. This allowed a static-fired ignitor average EPDM recession rate to the high-density char surface to be determined, through post mortem inspection, to be 3.7 mil sec^{-1}, in agreement with the arc tunnel radiation data of 1.9 mil sec^{-1} at half the radiative heating rate with no char loss. This indicates that the motor-case heat-transfer environment in the region of the ignitor is basically radiative (in spite of the 6000°R, 600-psi peak pressure combustor conditions, which certainly imply a uniform solid fuel burning process), and that the EPDM thickness appeared to be adequate for ignitor housing protection.

Table IV. EPDM-Viton Radiation Test Comparison

Material	Radiator Temp. (°R)	Density (lb ft^{-3})	$\dot{q}_c$(RAD) (Btu ft^{-2}sec^{-1}) (°R)	Sample Char Temp. (°R)	$\dot{S}$ (mil sec^{-1})	Q^* (Btu lb^{-1})
EPDM	5080	70	160	3300	1.9	~ 10,000
Viton	5080	114	160	3200	4.4	~ 3,000

Table V. EPDM-Viton Comparison Summary

Convection Heating $\dot{q}_{HW}$ = 140 Btu ft^{-2} sec^{-1}	Density (lb ft^{-3})	$\dot{S}$ (mil sec^{-1})	Q^* (Btu lb^{-1})
EPDM	70	15	~ 1,000
Viton	114	25	~ 400
Radiation Heating $\dot{q}_{RAD}$ = 160 Btu ft^{-2} sec^{-1}			
EPDM	70	1.9	~10,000
Viton	114	4.4	~ 3,000

In addition, char interface temperatures for both EPDM and Viton were also measured for high-heating-rate conditions to be ~ 2050°R. This contrasts with the low-heating-rate TGA analysis value of ~ 1060°R for both rubbers. This high-heating-rate interface temperature is required along with recession rate for heat transfer analyses through the thermal protection system. Experiment and analysis both converged to the conclusion that the ignitor housing thermal protection design appeared adequate. Thus scenario (2) was also deemed unlikely as a result of these ablation studies coupled with the static test firing results. However, because of a possible increase in the importance of the convection component of the heating environment at 2.4-g acceleration in flight relative to the 1-g static test condition, a 50% increase in EPDM thickness was made as a precautionary measure.

The high-heating-rate ablation properties of Viton rubber, used in a thermal boot located under the nose cap wing region to cover the suspect Techroll Seal, were shown to be inferior to EPDM in this study. However, no damage to the nose cap wing was ever observed in the static test firings, thus no severe radiative or convective heating of the Viton boot was experienced; hence concern for this aspect of the overall problem diminished. In addition, Viton is more resilient than EPDM and was therefore retained as the preferred boot material.

IV. GRAFOIL SEAL LEAKAGE

The bulk of the laboratory effort focussed on scenario (3), hot-gas
leakage past a grafoil seal, which emerged as the most probable scenario.
This study initially involved (1) arc tunnel simulation of an AEDC BS-1 base-
line firing condition which exhibited evidence of a grafoil seal leak of hot
SRM exhaust gases and an attendant temperature rise in the Techroll titanium
housing to a critical 1260°R, and later (2) simulation of worst-case hot-leak
heating rate conditions for more severe testing.

Exact simulation of the temperature and pressure histories and the chemi-
cal species makeup of the combustor gases was not possible with the facility
employed. Rather, after initial turn-on transient behavior, nominally fixed
temperature (3260 to 4060°R) and pressure (~ 90 psia) plenum operation was
employed in most tests using argon as the test gas. Average-value heating
rate over the nominal motor burn times was the governing simulation require-
ment for most of the test series. See Fig. 6 for a cross-sectional represen-
tation of the arc jet simulation of a grafoil seal hot-gas leak. Hot argon
from the arc heater flows through the 0.052-in.-diam nozzle to impinge upon
the 3-in. × 10-in. × 0.27-in. titanium plate (with a shear lip extension) in
simulation of the mass and dimensions in the shear lip region of the SRM
titanium housing. The temperature trace of a TC embedded in the titanium
plate, obtained during an arc jet calibration run, is shown in Fig. 7 along
with a TC trace from the AEDC BS-1 firing which exhibited a grafoil seal heat
leak. The close agreement of the two traces was considered to be a conserva-
tive simulation of the heating rate experienced in the BS-1 test firing.

After the heating rate calibration, design changes in the shear lip
region involving addition of EPDM and silica-phenolic (Si-P) slabs to the
titanium were evaluated. Early EPDM results directed attention away from this
material for thermal protection enhancement under the shear loading of a hot
gas jet, because the EPDM ablated rapidly. Worst-case simulation studies were
also implemented that involved larger mass flows through larger slit nozzles
(0.030-in. × 0.590-in. slot followed by 0.015-in. × 0.590-in. slot). Several
design-enhancement variations, including use of tantalum shields, shear lip
removal, etc., were investigated in the course of the study. Eleven titanium
housing thermal insulator candidate configurations were tested in a series of
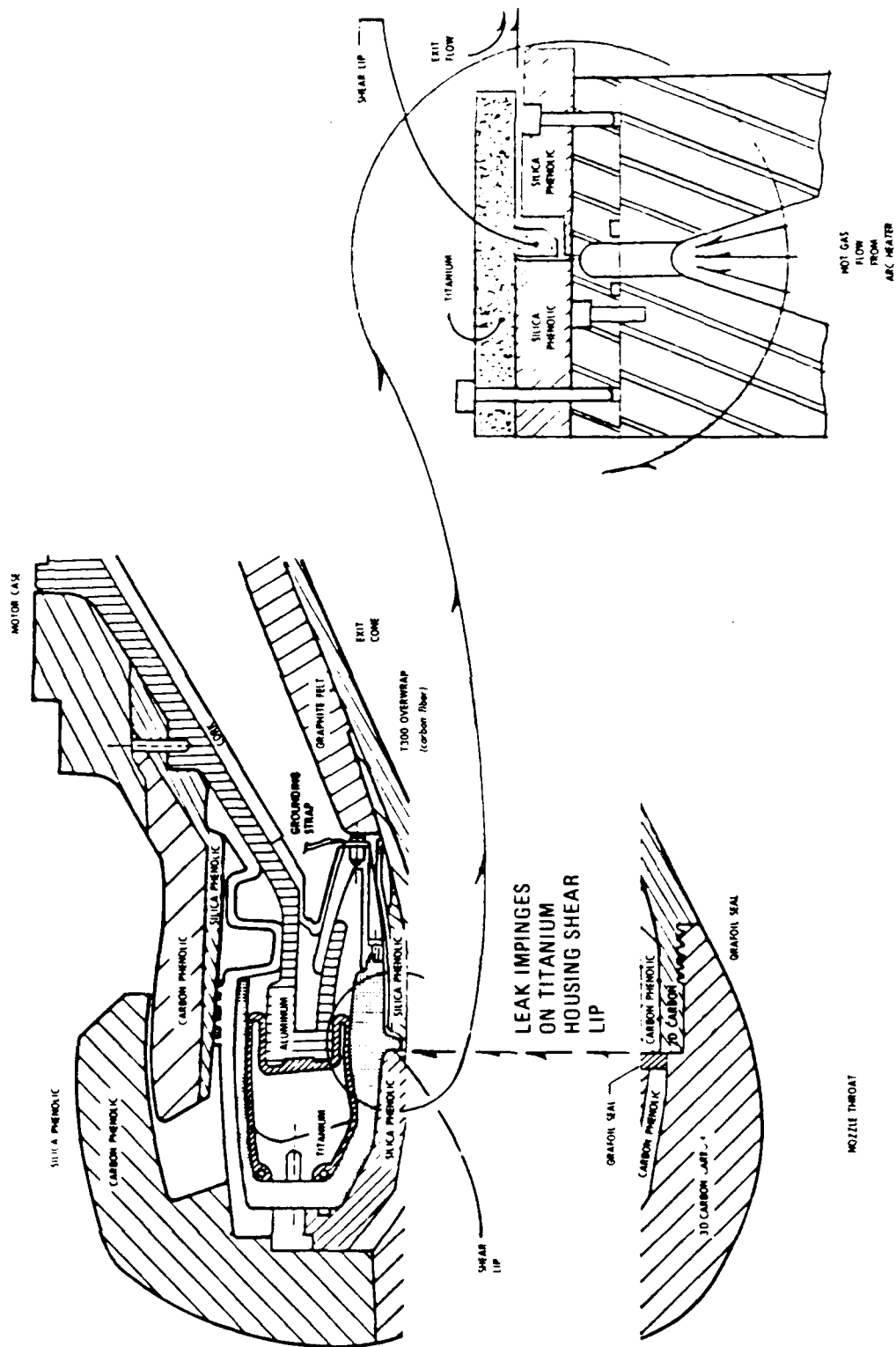
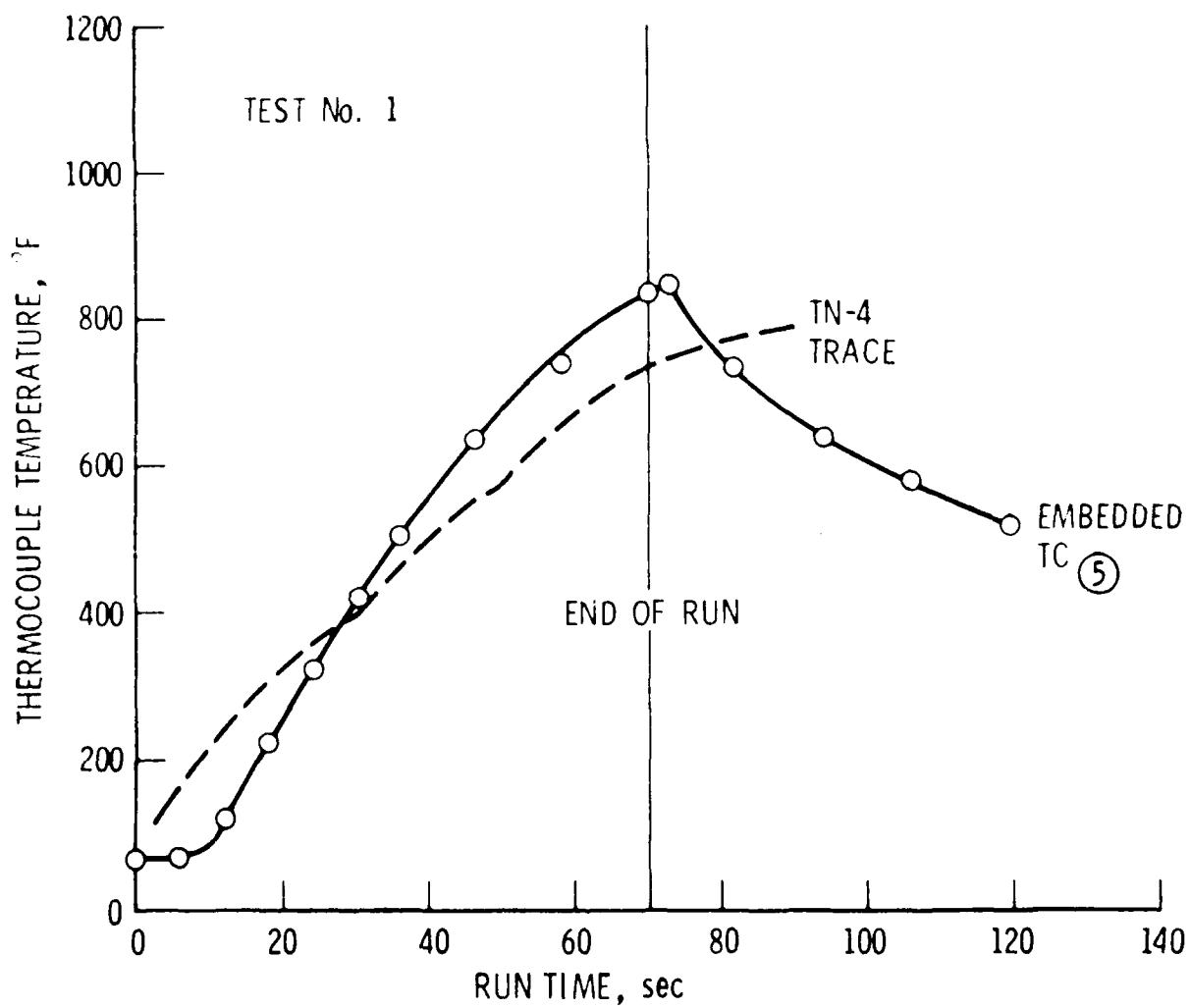Fig. 6. Arc jet simulation of grafoil seal hot-gas leak.

Fig. 7.   Arc-jet-heating calibration of titanium plate.

29 tests. Ultimately an enhanced design evolved which made use of a reduced shear lip protected by a 0.156-in.-thick Si-P overhang coupled with a Si-P insert on the titanium housing. It was shown to be adequate to preclude excessive temperature development in the titanium housing should a leak occur, yet it required minimal system impact and was thus selected for system implementation. Figure 8 illustrates the successful design for corrective action. This selected candidate design was implemented in AEDC firing tests where again it proved adequate (reducing critical Techroll Seal housing temperatures from ~ 800°F to 200°F at end of burn; see Table VI), and on the final successful flight hardware.
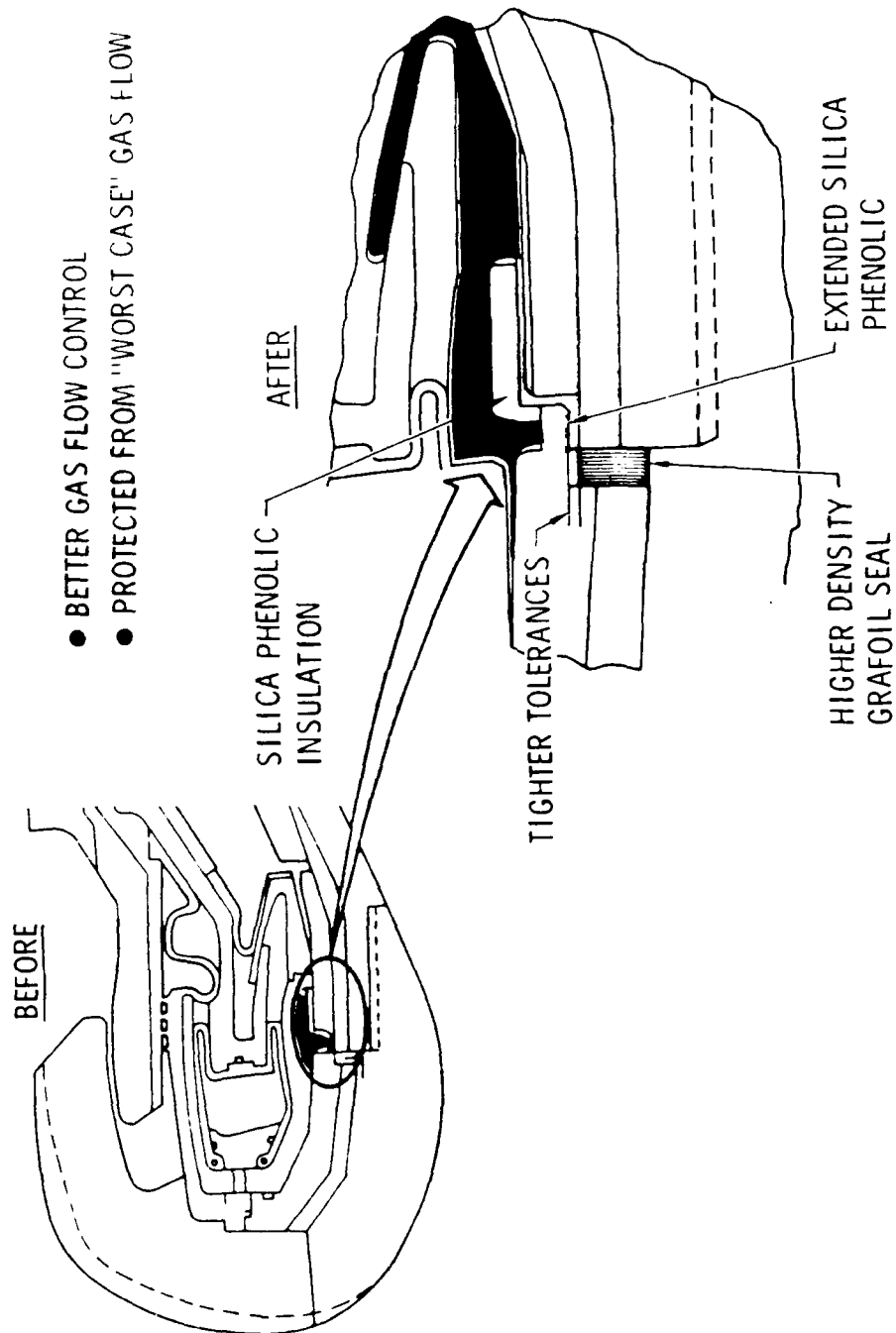
- BETTER GAS FLOW CONTROL
- PROTECTED FROM "WORST CASE" GAS FLOW

BEFORE

AFTER

SILICA PHENOLIC
INSULATION

TIGHTER TOLERANCES

EXTENDED SILICA
PHENOLIC

HIGHER DENSITY
GRAFOIL SEAL

Fig. 8.   SRM-2 nozzle corrective action.

Table VI. IUS/SRM-2 Static Test Firing Results at AEDC

29 Developmental and Qualification Tests			No Quench
BS-1	Baseline	800°F Peak Housing Temp.	Quench
FQ-1	Flight Qual.	460°F Peak Housing Temp.	Quench

All Changes Incorporated

WT-1	Witness Test	200°F Peak Housing Temp.	Quench
TMV-1	Thermal Margin Verification	200°F Peak Housing Temp.	Quench

V. CONCLUSION

This thermal test program illustrates the great utility and versatility of an arc tunnel for responding rapidly and effectively to the testing needs imposed by a high-priority/high-pressure program associated with resolution of rocket motor failure. Data were gathered relating to the three proposed failure scenarios and resulted in timely guidance and ultimately to resolution of the system problem through verification of viable, enhanced design-fix concepts.

REFERENCES

1. McCoy, K. E. and J. Hester, "Analytical investigation of solid rocket nozzle failure," NASA-TM-86513, Aug. 1985.

2. Pfannerstill, J. A., "Shuttle 51C mission report," <u>Spaceflight</u>, <u>27</u>, 364-366 (1985).

3. Bangsund, E. L. and S. R. Hannah, "IUS Status and Growth Potential," <u>Earth-Oriented Applications of Space Technology</u>, <u>4</u> (1), 1-8 (1984).

4. McCoy, K. E. and J. L. Vaniman, "IUS (Inertial Upper Stage)/SRM-2 Nozzle Thermal Assessment," JANNAF Rocket Nozzle Technology Subcommittee Meeting, Huntsville, AL, 4-6 Dec. 1984; AD-B089 972L, pp. 105-117.

5. Chang, I. S., "Inertial Upper Stage Three Dimensional Thermal Analysis," JANNAF Rocket Nozzle Technology Subcommittee Meeting, Huntsville, AL, 4-6 Dec. 1984; AD-B089 972L, pp. 65-98.

6. Chase, C. A. and D. A. North, "IUS Propulsion Status," AIAA/ASME/SAE 20th Joint Propulsion Conference, Cincinnati, OH, 11-13 June 1984; AIAA paper 87-1192.

7. Courtesy of I. S. Chang, The Aerospace Corporation.

The Aerospace Corporation functions as an "architect-engineer" for national security projects, specializing in advanced military space systems. Providing research support, the corporation's Laboratory Operations conducts experimental and theoretical investigations that focus on the application of scientific and technical advances to such systems. Vital to the success of these investigations is the technical staff's wide-ranging expertise and its ability to stay current with new developments. This expertise is enhanced by a research program aimed at dealing with the many problems associated with rapidly evolving space systems. Contributing their capabilities to the research effort are these individual laboratories:

Aerophysics Laboratory: Launch vehicle and reentry fluid mechanics, heat transfer and flight dynamics; chemical and electric propulsion, propellant chemistry, chemical dynamics, environmental chemistry, trace detection; spacecraft structural mechanics, contamination, thermal and structural control; high temperature thermomechanics, gas kinetics and radiation; cw and pulsed chemical and excimer laser development including chemical kinetics, spectroscopy, optical resonators, beam control, atmospheric propagation, laser effects and countermeasures.

Chemistry and Physics Laboratory: Atmospheric chemical reactions, atmospheric optics, light scattering, state-specific chemical reactions and radiative signatures of missile plumes, sensor out-of-field-of-view rejection, applied laser spectroscopy, laser chemistry, laser optoelectronics, solar cell physics, battery electrochemistry, space vacuum and radiation effects on materials, lubrication and surface phenomena, thermionic emission, photo-sensitive materials and detectors, atomic frequency standards, and environmental chemistry.

Computer Science Laboratory: Program verification, program translation, performance-sensitive system design, distributed architectures for spaceborne computers, fault-tolerant computer systems, artificial intelligence, micro-electronics applications, communication protocols, and computer security.

Electronics Research Laboratory: Microelectronics, solid-state device physics, compound semiconductors, radiation hardening; electro-optics, quantum electronics, solid-state lasers, optical propagation and communications; microwave semiconductor devices, microwave/millimeter wave measurements, diagnostics and radiometry, microwave/millimeter wave thermionic devices; atomic time and frequency standards; antennas, rf systems, electromagnetic propagation phenomena, space communication systems.

Materials Sciences Laboratory: Development of new materials: metals, alloys, ceramics, polymers and their composites, and new forms of carbon; non-destructive evaluation, component failure analysis and reliability; fracture mechanics and stress corrosion; analysis and evaluation of materials at cryogenic and elevated temperatures as well as in space and enemy-induced environments.

Space Sciences Laboratory: Magnetospheric, auroral and cosmic ray physics, wave-particle interactions, magnetospheric plasma waves; atmospheric and ionospheric physics, density and composition of the upper atmosphere, remote sensing using atmospheric radiation; solar physics, infrared astronomy, infrared signature analysis; effects of solar activity, magnetic storms and nuclear explosions on the earth's atmosphere, ionosphere and magnetosphere; effects of electromagnetic and particulate radiations on space systems; space instrumentation.